

PERFORMANCE OF THE REST2 MODEL FOR 1-MINUTE CLEAR-SKY SOLAR IRRADIANCE WITH MERRA-2 ATMOSPHERIC INPUTS

Paola Russo – paolarussoganon@gmail.com

Agustín Laguarda

Gonzalo Abal

Inti Piccioli

Laboratorio de Energía Solar, Universidad de la República, Uruguay

Abstract. The broadband irradiances (GHI, DHI, DNI) and the photosynthetically active radiation (PAR) estimated by the REST2 clear sky model are evaluated against 1-minute high quality ground measurements for one site representative of the Pampa Húmeda region of southeastern South America. The MERRA-2 reanalysis database is used to provide the required atmospheric inputs for the model (water vapor, aerosol content, ozone). Our results show an acceptable performance for GHI, DNI and PAR but a high uncertainty in the estimated DHI.

Keywords: Clear-sky models, solar irradiance, PAR.

1. INTRODUCTION

Clear sky models are essential for solar resource assessment. First, they can be used as a basis for satellite-based solar irradiance models under all-sky conditions (Laguarda *et al.*, 2020) or in solar forecasting applications (Marchesoni and Alonso-Suárez, 2020). Second, they are used in quality control of solar irradiance data (Perez-Asturillo, Bachour and Martin-Pomares, 2018) and for solar resource characterization (Russo, Abal and Laguarda, 2021).

Several broad-band clear-sky models have been proposed and are in use worldwide. A recent review of seventy models can be found in (Antonanzas-Torres *et al.*, 2019). These models require inputs describing the state of the atmosphere and produce one or more components of solar irradiance. The simplest models can use one effective input, such as the the ESRA model (Rigollier, Bauer and Wald, 2000) which is based on Linke Turbidity (Laguarda and Abal, 2016), and still provide hourly horizontal global irradiance with reasonable accuracy (Laguarda and Abal, 2020). More precise models use several atmospheric inputs and have the potential to achieve good accuracy, provided those inputs are available with the required time scales and with low uncertainty. This is not typically the case at most locations and one must resort to satellite-based estimates for atmospheric parameters such as water vapor or aerosol content.

One of the most detailed clear-sky models in use is REST2 (Gueymard, 2008), which is based on a parametrization of the radiative transfer model SMARTS2 (Gueymard, 2005). REST2 models solar beam irradiance attenuation in two broadband regions: band 1 (visible or VIS) at 290 - 700 nm and band 2 (infrared or IR) at 700-4000 nm. In the VIS region attenuation is mainly due to Rayleigh scattering by air molecules and scattering and absorption by aerosols. In the IR region, attenuation is mainly due to water vapor and other residual gasses in the atmosphere. The model produces estimates for direct normal irradiance (DNI), global horizontal irradiance (GHI), diffuse horizontal irradiance (DHI), PAR¹ irradiance and illuminance. It uses up to eight input variables (Gueymard, 2008). These variables are precipitable water vapor (w , cm), the Ångström turbidity parameters (α_1 , α_2 , β), local atmospheric pressure (p , hPa), ozone column (u_o , cm) and the ground scattering albedos for band 1 and band 2, ρ_{g1} and ρ_{g2} . The REST2 model allows generic values to be used when the local information is not available. Most relevant among these input variables are precipitable water vapor and the Ångström turbidity parameters describing the aerosol content. These can be obtained (for any site worldwide) from the reanalysis data base MERRA-2 (Gelaro *et al.*, 2017). This database combines satellite-based estimates with the atmospheric model Global Earth Observing System Version-5 (GEOS-5) to provide several atmospheric variables² at the hourly timescale (starting in 1980) on a grid of $0.5^\circ \times 0.625^\circ$ of latitude and longitude. Some of the variables in MERRA-2 have been evaluated against data from AERONET stations. In Gueymard and Yang (2020), AOD550 (aerosol optical depth at wavelength of 550 nm) and α are evaluated worldwide. In (Laguarda and Abal, 2020) precipitable water, aerosol content and ozone have been evaluated for the region of interest in this work, using three AERONET stations available.

¹ Photosynthetically Active Radiation, or global horizontal irradiance in the range 400-700 nm.

² MERRA-2 data is available at the Giovanni site hosted by NASA <https://giovanni.gsfc.nasa.gov/>.

In this work, the REST2 model is evaluated at the 1-min timescale against quality controlled ground data for one site (representative of the Pampa Húmeda region of southeastern South America) for GHI, DHI, DNI and PAR irradiances. Estimates from MERRA-2 are used to obtain the required input variables. Thus, the validation is for the REST2 model in the region of interest, when used with MERRA-2 inputs.

2. DATA

In order to validate the model, its irradiance outputs (GHI, DHI, DNI and PAR) are compared to ground measurements, which are described below. Current atmospheric conditions at the site are obtained from the MERRA-2 reanalysis database which is provided at 1-hour intervals with spatial resolution of approximately 50 km.

2.1 Ground measurements of solar irradiance

The ground measurements were collected by the Solar Energy Laboratory at its main site located in Salto, Uruguay (latitude -31.2827, longitude -57.9198, altitude: 56 m above sea level). This site is representative of the broader region "Pampa Húmeda", which includes the territory of Uruguay, the eastern portion of Argentina and southern Brazil. It is a homogenous region of plain grasslands with low elevations, classified as Cfa (temperate, hot summer without dry season) in the Köppen-Geiger classification (Peel, Finlayson and McMahon, 2007).

The measurements were recorded at 1 minute intervals. The 4-year period 2017-2020 is used, registering a wide range of climatic conditions. GHI and DHI were measured with Kipp & Zonen model CMP10 pyranometers (Class A, spectrally flat) with a ventilation/heating unit Kipp & Zonen, CVF4. The pyranometer for DHI is shaded by a shadow ball assembly mounted on a Kipp & Zonen SOLYS2 sun tracker. DNI was measured with a Kipp & Zonen CHP1 pyrliometer mounted on the same tracker. A secondary sun sensor actively corrects the fine tracking. PAR was measured (in $\mu\text{mol}/\text{m}^2\text{s}$) with a Kipp & Zonen PQS1 quantum sensor. PAR is converted from photonic flux units ($\mu\text{mol}/\text{m}^2\text{s}$) to irradiance units (W/m^2) using the equivalence $1 \mu\text{mol}/\text{m}^2\text{s} = 0.21964 \text{ W}/\text{m}^2$ obtained³ from the extraterrestrial standard solar irradiance spectrum (Wehrli, 1985). The data was acquired with a Fisher Scientific DT85 data logger. The measurement station also records atmospheric variables such as air temperature, relative humidity and atmospheric pressure. All measurements were acquired following good laboratory practices with weekly maintenance. The pyranometers and pyrliometers used for solar irradiance measurements were periodically calibrated at the LES laboratory, at least once every two years, according to the standards ISO 9847:1992 and ISO 9059:1990. The reference pyranometer (Kipp & Zonen CMP22) and pyrliometer (Kipp & Zonen CHP1) participate in international comparisons at least once every 4 years and are traceable to the World Radiation Reference (WRR) from the World Radiation Center (WRC). The estimated uncertainties for this dataset at 1-min level are 2 % for DNI, 3 % for GHI and DHI and 5 % for PAR, in all cases expressed relative to the daytime average of each measurement.

2.2 Atmospheric information (MERRA-2)

The atmospheric variables used from MERRA-2 are: aerosol optical depth at wavelength 550 nm (AOD550, unitless), aerosol Ångström parameter at wavelengths between 470-870 nm (α , unitless), total column ozone (O₃, in Dobson Units or DU) and total precipitable water vapor (WV, in kg/m^2). All variables are downloaded at 1-hour intervals for a box of 0.5×0.625 degrees centered in the latitude and longitude of Salto measurement station for the period 2017-2020. In a post-processing step, these variables are linearly interpolated to 1-minute intervals. The original units are converted to the units that REST2 requires as input: $w(\text{cm}) = \text{WV}(\text{kg}/\text{m}^2) * 0.10$ and $u_o(\text{cm}) = \text{O}_3(\text{DU}) * 0.001$. The Ångström Turbidity Coefficient is calculated using Ångström equation: $\beta = \text{AOD}_{550} * 0.55^\alpha$. Since the validation is to be performed under typical conditions, extreme values present in the atmospheric time series are excluded. The filters applied are: $0.2 < u_o < 0.35 \text{ cm}$, $w < 5 \text{ cm}$, $\alpha < 1.87$, $\beta < 0.35$. The data that satisfies these three conditions is used as input for the model. The superficial ultraviolet albedo (ρ_{g1} , unitless) and superficial infrared albedo (ρ_{g2} , unitless) were set to a constant value of 0.2, a default value for grasslands according to SMARTS (Gueymard, 2005). The nitrogen dioxide amount (u_n , cm) was set to a constant value of 0.0002, as recommended by Gueymard (2008).

The accuracy of MERRA-2 estimates has been evaluated by comparison to ground measurements of the Aerosol Robotic Network run by NASA⁴ (AERONET). Recently, Gueymard and Yang (2020) performed a worldwide-scale validation of the aerosol products of MERRA-2 using 15 years of AERONET observations at 3 hour time intervals. Laguarda and Abal (2020) have performed a validation for the region of interest of this work (Pampa Húmeda) of MERRA-2 precipitable water vapor, aerosol products and ozone at 1-hour intervals, while also discussing the sensitivity

³ Available at <https://www.nrel.gov/grid/solar-resource/spectra-wehrli.html>

⁴ <https://aeronet.gsfc.nasa.gov/>

of clear sky models to the uncertainties in each of these variables. The results of this evaluation, based on three AERONET sites in the area, are summarized in Table 1.

Table 1: Validation of MERRA-2 atmospheric variables for the Pampa Húmeda region against three AERONET sites. See (Laguarda and Abal, 2020) for the details.

metric	AOD ₅₅₀	water vapor (cm)	Ångström exponent α
rMBD (%)	17.5	7.1	-2.9
rRMSD (%)	33.4	11.2	26.8
Pearson correlation	0.72	0.95	0.36
# observations	40888	37024	38496
median	0.070	1.55	1.09

The aerosol product AOD550 shows high dispersion, low correlation and a significant positive bias in the region. Water vapor has an acceptable dispersion with a significant positive bias. Thus, MERRA-2 estimates tend to systematically overestimate the aerosol and water vapor contents of the local atmosphere.

2.3 Quality control

Strict quality control procedures were applied to the ground measurements. The filtering procedure proposed in (Perez-Asturdillo, Bachour and Martin-Pomares, 2018) describes the seventeen filters that have been applied to the data. These filters include the Baseline Solar Radiation Network (BSRN) quality control recommendations (McArthur, 2005), supplemented with additional constraints to detect, for example, tracker mis-alignment conditions. Two additional filters were applied. A minimum solar altitude $\alpha_{\min} = 7^\circ$ was required, in order to minimize the directional (cosine) errors that affect pyranometers mainly at low solar altitudes. PAR was required to satisfy the upper and lower bounds (Opálková *et al.*, 2018);

$$PAR > 0.35 \times PAR_{TOA} \quad \& \quad PAR < 0.8 \times PAR_{TOA} - 51.615 \text{ W/m}^2, \quad (1)$$

where PAR_{TOA} is the solar irradiance on a horizontal plane at the top of the atmosphere in the wavelength range 400-700 nm⁵.

A summary of the quality control results for each variable (GHI, DHI, DNI, PAR) is shown in Table 2. The data records that passed the quality control are shown in Fig. 1 as blue dots.

Table 2: Quality control results for each variable. In the second row, in parenthesis, the % of the previous row.

variable	GHI	DHI	DNI	PAR
diurnal, non-null	1034546	1030765	1022205	1042128
pass relevant filters	767052 (74.1%)	767217 (74.4%)	752860 (73.7%)	864762 (83.0%)
clear sky samples	71603 (9.3%)	71603 (9.3%)	71603 (9.5%)	67096 (7.8%)

2.4 Clear sky selection algorithm

The validation requires a clear sky dataset for each model's output. Clear sky conditions were selected from the GHI time series using the method proposed by Reno and Hansen (2016), available at the Python library PVlib

⁵ This quantity is calculated as $PAR_{TOA} = G_{s, PAR} \cdot \cos(z) \cdot F_n$, where F_n is the orbital correction factor, z is the solar zenith angle and $G_{s, PAR} = 530 \text{ W/m}^2$ is the solar constant for the wavelength range 400-700 nm, obtained from integration of the extraterrestrial standard solar irradiance spectrum (Wehrli, 1985) between those wavelengths.

(detect_clearsky)⁶. It requires modeled clear sky estimates as ancillary information. The ESRA clear-sky model (Rigollier, Bauer and Wald, 2000) for GHI was used, with a locally determined Linke Turbidity T_L cycle (Laguarda and Abal, 2016). Strict parameters were used in the PVlib function to minimize false positives (i.e. data with thin clouds detected as clear sky).

In order to remove a few data points with high diffuse fractions ($f_d = \text{DHI}/\text{GHI}$) typical of cloudy conditions two additional conditions are imposed on the preliminary clear-sky data,

$$f_d < 0.6 \quad \& \quad f_d < 1 - k_t, \quad (2)$$

where $k_t = \text{GHI}/(G_0 \cos z)$ is the clearness index (the global horizontal irradiance normalized by the corresponding extraterrestrial value), G_0 is the extraterrestrial irradiance (including the orbital correction factor) and z is the solar zenith angle. This condition represents a trapezoidal region in Fig. 1, within which the clear sky data is located.

The number of clear sky measurements selected by this procedure⁷ is shown in the last row of Table 2. The final set of 1-min clear sky data is shown (orange dots) in the dimensionless diagram ($f_d - k_t$) presented in Fig. 1. The selected clear sky minute data will be used for the validation.

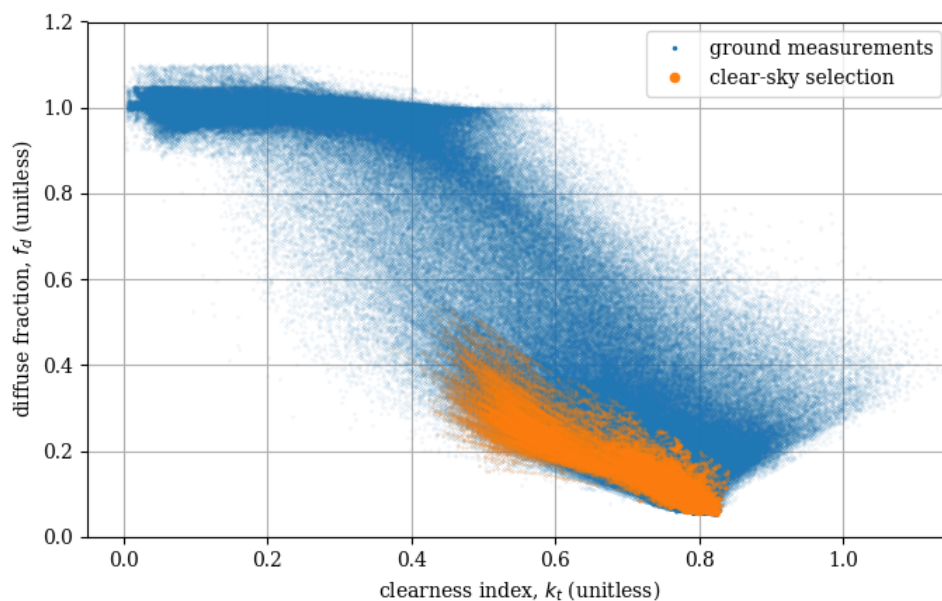


Figure 1: Diffuse fraction vs. clearness index ($f_d - k_t$) diagram, ground quality checked measurements (blue dots) and clear-sky selection (orange dots).

3. PERFORMANCE OF THE REST2 MODEL

The performance assessment of the REST2 model is done using the usual metrics: the mean bias deviation (MBD), the root mean square deviation (RMSD), the Kolmogorov-Smirnov integral (KSI) and the Pearson correlation. The first two measure the average bias and the average dispersion of the residuals between the estimates and the measurements, respectively. The KSI is a statistical similarity index based on the distance between the cumulative probability distributions of the measurements and the estimates (see, for example, Espinar *et al.*, 2009). In this work, the MBD, RMSD and KSI are expressed as a percentage, relative to the relevant measurement mean (i.e. rMBD, rRMSD and rKSI). Detailed definitions for these metrics, as well as examples of their use in solar resource assessment, can be found in (Gueymard, 2014).

3.1 Previous validations for REST2

Several validations of GHI, DNI and DHI from the REST2 model have been done in different parts of the world. The sites studied are mainly located in Europe, North America, North Africa, the Middle East, and - more rarely- in the Southern Hemisphere or South America. At the 1-minute level, the validations carried out by Gueymard (2012);

⁶ Documented at https://pvlib-python.readthedocs.io/en/stable/generated/pvlib.clearsky.detect_clearsky.html. The parameters used on the pvlib function were: window length = 10, slope deviation = 5, var_diff = 0.003, upper line length = 8, lower line length = 4.

⁷ The PAR data had some clear sky samples manually removed due to known shading events affecting the PAR sensor.

Engerer and Mills (2015) and Antonanzas-Torres *et al.* (2019) stand out, because they are recent, for temperate climates (such as the region of interest in this work), and because the three components of irradiance are considered (except for Engerer and Mills (2015), which omits DHI). Table 3 shows the average results from these studies in terms of rMBD and rRMSD.

These works compare a large number of clear sky models and all of them rank REST2 between those with the highest performances. Gueymard (2012) validates REST2 estimates with AERONET atmospheric information over 4 measurement's sites in the USA and one in Saudi Arabia. The validation, on a scale of 1-3 minutes, concludes that good models can estimate GHI with precision close to that of measurement instruments, being the DNI the most complex to model due to its strong dependence on aerosols contents. Engerer and Mills (2015) carry out a validation study of 9 models at 14 sites in Australia on a minute scale using interpolated atmospheric mean values extracted from the SoDa dataset (Rigollier, Lefevre and Wald, 2001). Antonanzas-Torres *et al.* (2019) carried out an extensive validation of 70 clear sky models at two BSRN stations in Europe at the 1-minute level. The aerosol optical depth and water vapor content information is obtained from local AERONET measurements.

Table 3: Performance metrics for REST2 estimates at 1-minute level on previous validations worldwide.

Study/variable	GHI		DHI		DNI	
	rMBD (%)	rRMSD (%)	rMBD (%)	rRMSD (%)	rMBD (%)	rRMSD (%)
Gueymard, 2012	-0.2	1.5	-0.4	8.8	-0.3	1.4
Engerer and Mills, 2015	+0.3	5.1	–	–	-0.3	5.2
Antonanzas <i>et al.</i>, 2019	-0.4	3.1	-1.0	5.8	-0.3	7.9

The results in Table 3 show that when the model is used with good quality atmospheric in-situ information it can provide high accuracy, similar to the accuracy of the measurement instruments.

In the region of interest of this work, a previous validation was performed at the hourly scale (Laguarda, 2021) using MERRA-2 atmospheric information and a smaller time span (2015-2017). For GHI, the model's estimates present a rMBD of -0.9% and a rRMSD of 3.6%. For DNI, a rMBD of -4.9% and a rRMSD of 7.2%. Another validation for DNI from REST2 (among other models) was done in (Porfirio and Ceballos, 2013) for three sites in northeastern Brazil (Petrolina, Natal and São Luis) using atmospheric inputs from the MODIS and OMI instruments⁸ from NASA. On average, the rMBD was +1.6 % and rRMSD was 3.2 % for DNI. Very sparse information was found on PAR validation, not making it possible to show the MBD and RMSD from temperate sites. At the best of our knowledge, DHI or PAR estimates of REST2 have not been validated in the region of interest.

3.2 Results

The performance metrics of the validation for the Pampa Húmeda site are presented in Table 4. GHI estimates show strong agreement with the measurements, resulting in a small underestimation and a rRMSD of 4%, similar to the typical uncertainty of a pyranometer's measurement. The performance of the PAR estimates is similar to GHI, but with a slightly positive bias. In both cases the correlation is very high (greater than 0.99) and the relative KSI less than 2%. On the other hand, the model with MERRA-2 inputs has difficulties to estimate DHI accurately. The overestimation of this variable is very high (in relative terms 40% of the mean) and the dispersion is near 50%, although in absolute terms its RMSD is 35.1 W/m², similar to the other variables (RMSD around 16 W/m² for PAR and 25 W/m² for GHI). The low mean of clear-sky DHI accounts for the high values in relative terms. In addition, the estimate-measurement correlation for DHI is weaker, with a value around 0.8. In the case of DNI, the model clearly underestimates and its dispersion is of the order of 8% of the mean. However, this variable presents a good correlation and a low KSI. These results can be seen in the scatter plots shown in Fig. 2. There is a good agreement between GHI and PAR measurements and estimates. It is evident that the dispersion is greater for DHI and DNI than for GHI and PAR. It is also clear that the model presents great uncertainty to estimate DHI, which under clear sky conditions has low values, typically between 10-15% of GHI. The REST2 model with MERRA-2 inputs clearly underestimates DNI while overestimating DHI.

⁸ MODIS = Moderate Resolution Imaging Spectroradiometer, <https://modis.gsfc.nasa.gov/>
OMI = Ozone Monitoring Instrument, <https://aura.gsfc.nasa.gov/omi.html>

The current validation using MERRA-2 presents higher biases when compared to the validations presented in Table 3, which use AERONET measurements as atmospheric inputs. This may be due to the accuracy of the MERRA-2 reanalysis dataset over the region of interest. The regional validation of this database (see Table 1) shows significant positive biases in AOD and water vapor. This implies greater atmospheric turbidity, which leads to an underestimation of DNI and an overestimation of DHI, as noted in Laguarda and Abal, (2020). These two deviations of opposite sign are attenuated in the estimation of GHI and PAR, which is only slightly underestimated.

Table 4: Performance metrics for REST2 estimates.

metric/variable	GHI	DHI	DNI	PAR
rMBD (%)	-1.8	+39.9	-5.5	+1.0
rRMSD (%)	3.7	48.3	8.4	5.1
correlation	0.9982	0.8421	0.9623	0.9941
rKSI (%)	1.9	18.1	7.8	1.7
average (W/m ²)	666.0	72.7	838.9	310.1

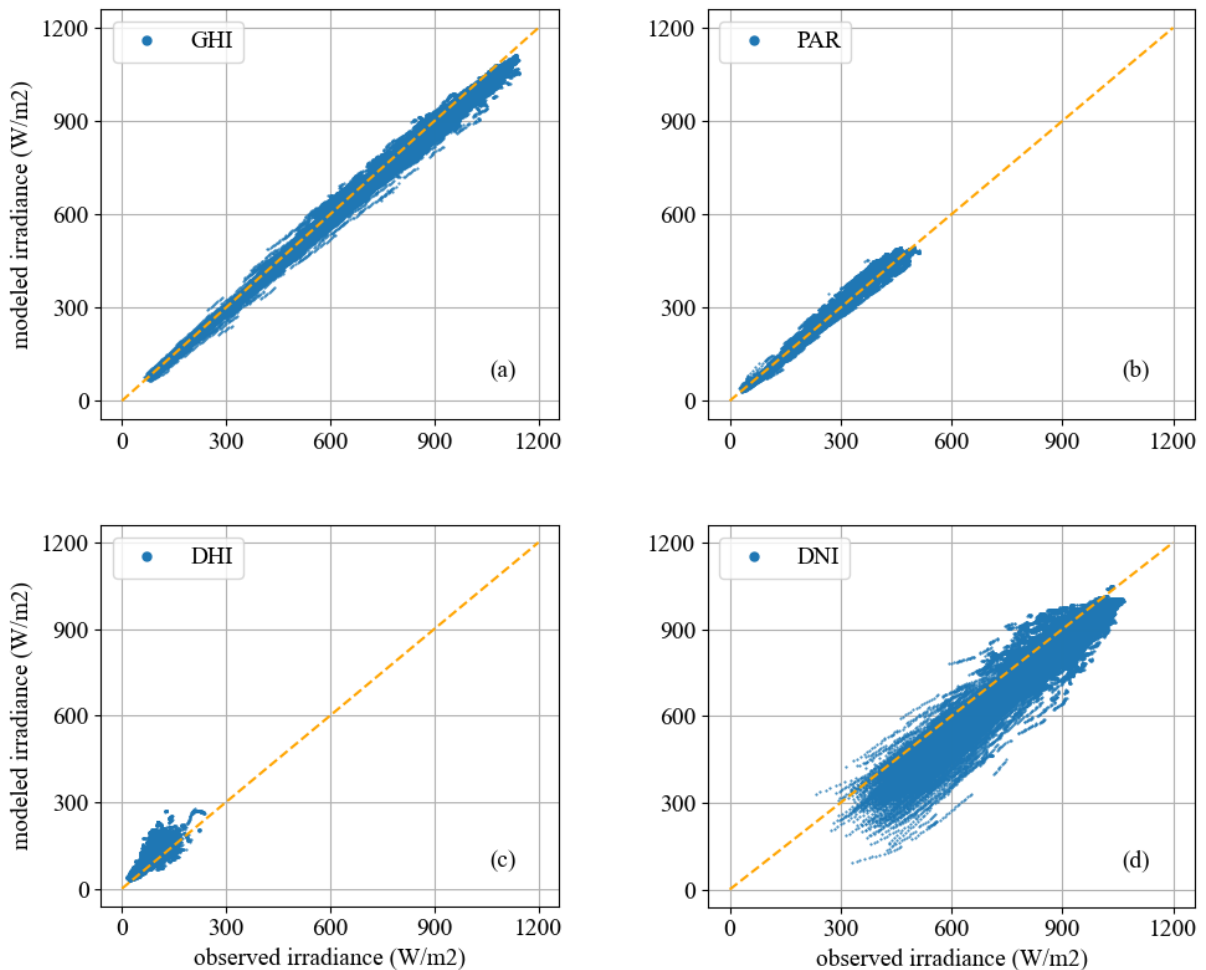
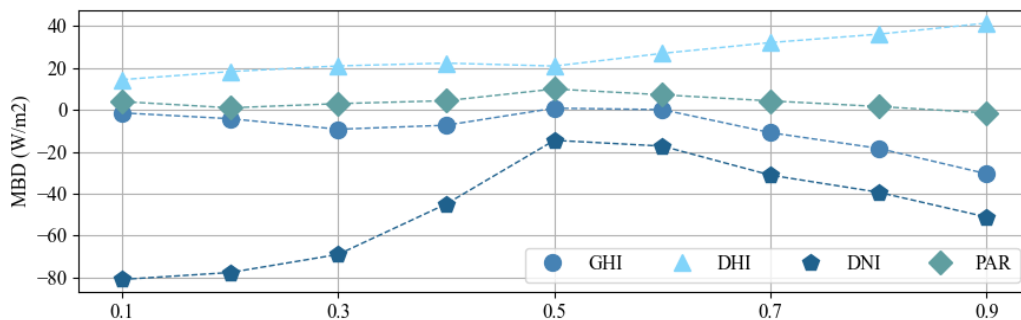


Figure 2: Model performance compared to ground measurements for GHI, DHI, DNI and PAR.

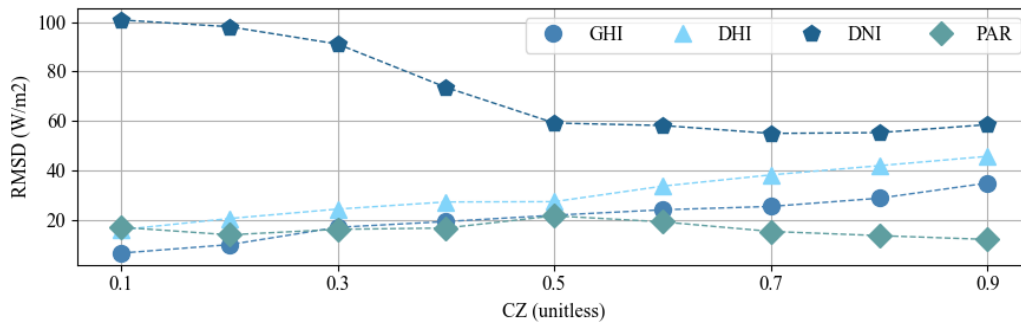
3.3 Dependence of the 1-min deviations with solar zenith angle

In order to study the error in terms of solar altitude (or air mass), the dependence of MBD and RMSD (in absolute terms) with the cosine of the zenith angle⁹ (CZ) is analyzed. Higher CZ values are associated with solar noon, while lower values are associated with low solar altitudes and high relative air mass. Figure 3(a) shows that the model systematically overestimates DHI for all solar altitudes, being the effect more marked for CZ greater than 0.6. On the other hand, DNI is underestimated for all values of CZ, but specially for CZ lower than 0.5 (low sun). As expected, these deviations of opposite sign partially cancel in the estimation of GHI, which shows small negative bias increasing towards solar noon. PAR shows the lowest bias and it is stable for all solar altitudes.

Figure 3(b) shows the dependence of the RMSD with CZ. For DHI, GHI and PAR, the dispersion grows gradually with CZ. The accuracy of DNI estimates show a marked dependence on CZ. The dispersion is high at low CZ (higher air mass) and it stabilizes at a low value for CZ greater than 0.5 (low air mass). This reflects the fact that REST-2 models DNI using a product of atmospheric transmittances, an approximation which is less accurate at high air masses.



(a) MBD vs CZ



(b) RMSD vs CZ

Figure 3: Absolute MBD and RMSD vs the Cosine of Solar Zenith angle for DHI, DNI, GHI and PAR.

4. CONCLUSIONS

The high-performance solar radiation model for cloudless-sky broadband irradiance and photosynthetically active radiation, REST2, is implemented and evaluated over one site in Northern Uruguay representative of the broader Pampa Húmeda region in Southeastern South America. The model requires up to 8 input atmospheric parameters, of which the most relevant are water vapor, aerosol optical thickness and the Angström exponent. These variables were obtained from the MERRA-2 reanalysis database. The validation was performed at the 1-minute timescale using clear sky measurements automatically selected by an algorithm from 4 years of controlled quality ground data. The validation includes the four irradiance outputs of the model, GHI, DHI, DNI and PAR.

Over the region of interest, REST2 used with MERRA-2 inputs can estimate GHI and PAR with a typical uncertainty (in terms of rRMSD) of 4% and 5% of the mean, respectively. On the other hand, DNI can be estimated with a typical uncertainty of 8%. When modeled DNI is used, it should be considered that this variable presents a

⁹ This quantity is related to the solar altitude ($\sin \alpha = \cos z$) and to the relative air mass, $m = 1/\cos z$.

negative bias, mainly at low solar altitudes or high air mass. Finally, DHI, a variable with a secondary role under clear sky conditions, is estimated with high relative uncertainty (48%) and shows an important over-estimation of 40%.

Previous studies suggest that REST2 can present very high precision when used with high quality aerosol and water vapor in situ measurements, usually from AERONET sites. This information is not available for most locations, thus it is relevant to assess the model using MERRA-2 reanalysis data, which is available worldwide at 1 hour intervals. In the region of study, the MERRA-2 database tends to overestimate the aerosol optical thickness and the precipitable water vapor content. As noted in previous works, this results in a systematic under-estimation of DNI and an over-estimation of DHI. These effects partially cancel and result in a small underestimation of GHI. On the other hand, the data from MERRA-2 base captures the intraday variability of the atmosphere, and this makes it useful for capturing the small variations of the solar components with accuracy, provided a post-processing (local adaptation) is applied to the initial estimates. In further studies these improvements in the atmospheric information and also data from the surface albedo (that can affect mainly the DHI) will be studied to improve the performance of the model. These simple procedures are expected to significantly reduce the bias and improve the overall performance of the REST2 model when used with MERRA-2 inputs.

Acknowledgements

The authors acknowledge financial support from CSIC/UDELAR (Uruguay) under project #117. The authors would like to thank the Solar Energy Laboratory staff for providing the data for this work, in particular Prof. José Di Laccio for generating the PAR constant and Tech. Andrés Monetta for his dedicated work in data acquisition.

REFERENCES

- Antonanzas-Torres, F., Urraca, R., Polo, J., Perpiñán Lamigueiro, O., and Escobar, R., 2019. Clear sky solar irradiance models: A review of seventy models. *Solar Energy, Renewable and Sustainable Energy Reviews*: pp. 374–387. DOI: 10.1016/j.rser.2019.02.032
- Engerer, N.A., Mills, F.P., 2015. Validating nine clear sky radiation models in Australia. *Solar Energy*, vol. 120. pp 9-24, ISSN 0038-092X. DOI:10.1016/j.solener.2015.06.044
- Espinar, B., Ramírez, L., Drews, A., Beyer, H. G., Zarzalejo, L. F., Polo, J., Martín, L., 2009. Analysis of different comparison parameters applied to solar radiation data from satellite and German radiometric stations. *Solar Energy*, vol. 83, pp. 118-125. DOI: 10.1016/j.solener.2008.07.009
- Gelaro, R., McCarty, W., Suárez, M., Todling, R., Molod, A., Takacs, L., Randles, C., Darmenov, A., Bosilovich, M., Reichle, R., y Wargan, K., 2017. The Modern-Era Retrospective Analysis for Research and Applications, Version 2 (MERRA-2). *Journal of Climate*, vol. 30, pp. 5419–5454. DOI: 10.1175/JCLI-D-16-0758.1
- Gueymard, C.A., 2005. SMARTS code, version 2.9.8 User's Manual. Solar Consulting Services. Available at <https://www.nrel.gov/grid/solar-resource/assets/data/smarts295-users-manual-pc.pdf>
- Gueymard, C.A., 2008. REST2: High-performance solar radiation model for cloudless-sky irradiance, illuminance, and photosynthetically active radiation – validation with a benchmark dataset. *Solar Energy*, vol. 82, pp. 272-285. DOI: 10.1016/j.solener.2007.04.008
- Gueymard, C.A., 2012. Clear-sky irradiance predictions for solar resource mapping and large-scale applications: Improved validation methodology and detailed performance analysis of 18 broadband radiative models, *Solar Energy*, vol. 86, issue 8, 2012, pp. 2145-2169. DOI: 10.1016/j.solener.2011.11.011
- Gueymard, C.A., 2014. A review of validation methodologies and statistical performance indicators for modeled solar radiation data: Towards a better bankability of solar projects. *Renewable and Sustainable Energy Reviews*. Elsevier Ltd. DOI: 10.1016/j.rser.2014.07.117
- Gueymard, C.A. and Yang, D., 2020. Worldwide validation of CAMS and MERRA-2 reanalysis aerosol optical depth products using 15 years of AERONET observations, *Atmospheric Environment*, p. 225. DOI: 10.1016/j.atmosenv.2019.117216
- Laguarda, A. and Abal, G., 2016. Índice de turbidez de Linke a partir de irradiación solar global en el Uruguay. *Avances en Energías Renovables y Medio Ambiente (AVERMA)*, vol. 20, pp 11.35-11.46. Available at http://les.edu.uy/papers/AVERMA2016_turbidez-Linke-Uruguay.pdf
- Laguarda, A. and Abal, G., 2020. Impacto de la incertidumbre de las variables atmosféricas de la base MERRA-2 en el modelado de la irradiancia solar en cielo despejado. *Avances en Energías Renovables y Medio Ambiente (AVERMA)*, vol. 24 (edición especial), pp 212-222. <https://avermaexa.unsa.edu.ar/index.php/averma/article/view/25>
- Laguarda, A., G. Giacosa, G., Alonso-Suárez, R. and Abal, G., 2020. Performance of the site-adapted CAMS database and locally adjusted cloud index models for estimating global solar horizontal irradiation over the Pampa Húmeda. *Solar Energy*, vol. 199, pp. 295-307. DOI: 10.1016/j.solener.2020.02.00

- Laguarda, A., 2021. Modelado de la irradiancia solar sobre la superficie terrestre: Modelos físicos e híbridos utilizando información satelital sobre la Pampa Húmeda. Tesis de Doctorado en Ingeniería de la Energía, Facultad de Ingeniería, Universidad de la República.
- Marchesoni, F. and Alonso-Suárez, R., 2020. Intra-day solar irradiation forecast using RLS filters and satellite images. *Renewable Energy* 161 (2020) 1140-1154. DOI: 10.1016/j.renene.2020.07.101
- McArthur, L., 2005. Baseline surface radiation network operations manual. Technical Report WCRP-121/ WMO. TD-No. 1274, World climate research programme–WMO.
- Opálková, M., Navrátil, M., Spunda, V., Blanc, P., Wald, L., 2018. A database of 10 min average measurements of solar radiation and meteorological variables in Ostrava, Czech Republic. *Earth System Science Data*, 10(2), 837-846. DOI: 10.5194/essd-10-837-2018
- Peel, M.C., Finlayson, B.L., McMahon, T.A., 2007. Updated world map of the Köppen-Geiger climate classification. *Hydrology and Earth System Sciences* 11, 1633–1644. DOI: 10.5194/hess-11-1633-2007
- Perez-Astudillo, D., Bachour, D., and Martin-Pomares, L., 2018. Improved quality control protocols on solar radiation measurements, *Solar Energy*, vol. 169, pp. 425–433. DOI: 10.1016/j.solener.2018.05.028
- Porfirio, A. C. S. and Ceballos, J.C., 2013. Um método de estimativa de irradiação solar direta normal a partir de imagens de satélite geostacionário: resultados preliminares, *Anais XVI Simpósio Brasileiro de Sensoriamento Remoto - SBSR*, pp. 6471-6479; Porfirio A. C. S., 2012. Estimativa de irradiação solar direta normal mediante satélite: um estudo para o Nordeste Brasileiro. Tese doctoral INPE (São José dos Campos) sid.inpe.br/mtc-m19/2012/08.09.17.57 - TDI.
- Reno, M.J. y Hansen, C.W., 2016. Identification of periods of clear sky irradiance in time series of GHI measurements. *Renewable Energy*, Vol.90, p. 520-531. DOI: 10.1016/j.renene.2015.12.031
- Rigollier, C., Bauer, O., and Wald, L., 2000. On the clear sky model of the ESRA (European Solar Radiation Atlas) with respect to the Heliosat method. *Solar Energy*, vol. 68, pp. 33–48. DOI: 10.1016/S0038-092X(99)00055-9
- Rigollier, C., Lefevre, M., Wald, L., 2001. Heliosat version 2. Integration and Exploitation of Networked Solar Radiation Databases for Environment Monitoring (SoDa Project). Tech. rep. URL <http://soda-is.com>.
- Russo, P., Abal, G. and Laguarda, A., 2021. Characterization of Solar Over-Irradiance Events in Uruguay. Full paper submitted to ISES Solar World Congress, 25-29 October 2021.
- Wehrli, C., 1985. Extraterrestrial Solar Spectrum, Publication no. 615, Physikalisch-Meteorologisches Observatorium. World Radiation Center, Davos Dorf, Switzerland, July 1985.